Cement & Concrete Composites 37 (2013) 2–11

Contents lists available at SciVerse ScienceDirect

Cement & Concrete Composites

journal homepage: www.elsevier.com/locate/cemconcomp

Carbon nanotube cement-based transducers for dynamic sensing of strain

Annibale Luigi Materazzi, Filippo Ubertini *, Antonella D'Alessandro

Dept. of Civil and Environmental Engineering, University of Perugia, Perugia, Italy

ARTICLE INFO

Article history:
Received 27 July 2012
Received in revised form 10 December 2012
Accepted 21 December 2012
Available online 7 January 2013

Keywords:
Smart concrete
Nanotechnology
Carbon nanotubes
Concrete structures
Monitoring

ABSTRACT

A new type of sensor for structural health monitoring (SHM) has emerged since the birth and development of nanotechnology and is based on cementitious materials additioned with carbon nanoparticles that can provide measurable electrical responses to applied strain. The response of similar transducers was mainly investigated under slowly varying strains while applications in dynamics have not been yet documented.

This paper is aimed at exploring the applicability of carbon nanotube–cement based sensors for measuring dynamically varying strain in concrete structures. Experiments are presented to investigate the electrical response of prismatic specimens made of carbon nanotube–cement composite when subjected to sinusoidal stress–strains in the typical frequency range of large civil structures. The results demonstrate that the sensors' output retains all dynamic features of the input thus providing useful information for SHM and encouraging the transformation of structures into infinite sets of potential sensors with enhanced durability and limited access issues.

1. Introduction

In the last decade, nanotechnology was successfully applied to cementitious materials, enhancing some of their traditional properties, such as durability and strength, while also introducing new capabilities of the material. From this perspective, the addition of nanomaterials to traditional admixtures seems promising and could include carbon nanotubes and nanofibers, which are known to be capable of providing cementitious materials with a "strain-sensitive" property. In particular, this new class of modified "strain-sensitive" cementitious materials can detect changes in mechanical strain acting upon them, outputting variations in their electrical properties, such as their resistance and reactance.

Because cementitious matrices are essentially non-conductive, sensitivity to strain variations with respect to changes in electrical resistance can often be achieved using even a relatively small amount of nanoadditives.

Much of the literature on this topic has studied the correlation between strain and electrical properties from both theoretical and the experimental points of view. Most of these experiments have discovered very complex behavior, indicating that the investigated physical phenomena involved many causes of nonlinearity and concluding that further studies are necessary before practical applications of such materials can take place. Although such efforts are still in progress, the studies up to this point have focused mainly on the behavior of these materials under static loads. On the contrary, experiments on the response of these materials to time-varying loads have been rare in the literature.

The aim of this paper is to exploit the already known strain-sensing ability of carbon nanotube–cement composites for manufacturing transducers able to provide dynamic measurements of strain in concrete structures. To this purpose, experiments were carried out to investigate the electrical response of prismatic specimens of cement paste prepared with carbon nanotubes when subjected to sinusoidal axial loads covering the typical frequency range of vibration of large civil engineering structures. The study was a part of a research program recently started by the authors that has yielded encouraging results in a recent study [1], which, after optimizing the mix design of a cement paste with carbon nanotubes, found a clear correlation between electrical resistance and axial strain in static load cases.

The paper is organized as follows. Section 2 presents an up-to-date survey of the literature devoted to self-sensing fiber-reinforced cementitious materials. Section 3 states objectives and motivations of the work in light of prior related literature studies along with a brief discussion of the potential for cement-based nanotechnology-modified sensors. The experimental procedures to investigate the correlation between electrical resistance and applied time-varying stress are presented in Section 4. The results of the experimental tests are analyzed and discussed in Section 5.

* Corresponding author. Tel.: +39 075 585 3954; fax: +39 075 585 3897.
E-mail address: ubertini@unipg.it (F. Ubertini).

0958-9465/$ - see front matter © 2013 Elsevier Ltd. All rights reserved.
http://dx.doi.org/10.1016/j.cemconcomp.2012.12.013

2. Literature review on nanotechnology-modified cement-based sensors

Cement-based composites are quasi-brittle materials exhibiting electrical and heating insulation features. Many properties of cementitious materials are affected by their micro- and nanobehavior [2,3]. Typical cementitious material reinforcements use fibers and microfibers. The development of new nanosized fibers, such as carbon nanotubes (CNTs), has opened up a new field for nanoreinforced concrete [4–8]. The remarkable mechanical and electrical properties of CNTs suggest that they are ideal candidates for creating smart cementitious composites. However, the problem of providing good fiber dispersion has become an essential issue requiring serious consideration and resolution [9].

Among the promising and innovative applications of smart nanomodified cementitious materials are strain-sensitive sensors based on cementitious materials. "Strain-sensitive" materials are those capable of feeling changes to their resistance through the use of peculiar inherent capabilities without destructive investigations. This self-monitoring function is achieved by correlating the variation of the applied stresses with the variation of appropriate parameters and properties of the material, primarily the electrical resistance. The deformation or tension state can be estimated through the resistance or electrical resistivity changes allowing the emergence and spread of damage and microfractures to be monitored. In some cases, this property was also used to create coatings made of strain-sensitive composite materials and applied on the surface of the monitored structures [10–13].

The most suitable self-monitoring materials for these purposes are non-conductive fiber-reinforced cementitious and composite materials. In fact, a non-conductive or poorly conductive matrix has greater sensitivity to changes in electrical resistance.

Earliest contributions about self-sensing concrete [14] have concerned cementitious materials reinforced with glass and carbon fibers. Fu and Chung [6] have researched the strain sensitivity of carbon fiber-reinforced cement compared to that of normal cement since 1993. Methyl cellulose, latex and silica fume were used to help the fibers disperse: otherwise, particles were treated on their surface. The samples were two-inch-square cubes subjected to compression cycles or fatigue [6], prisms with a square base of 4×4 cm and 16 cm long subjected to bending or impact tests [15] or a variety of different shapes including bone-shaped specimens for tensile tests and cross-shaped samples with variable sections [16–22]. The electrical resistance of matrices without any fiber was found to vary only after breaking because of the lower air conductivity with respect to that of the matrix. The fiber-reinforced matrix instead showed an increase in resistivity up until rupture and a subsequent decrease due to the conductivity of the fibers alone. This sensitivity has been attributed to the effect of carbon fiber pull-out during the opening of cracks because it tends to decrease the amplitude of the cracks, causing a consequent increase in resistivity of the contact between matrix and fibers [4].

In the case of cyclic loads, the fiber-reinforced materials have shown an increase in electrical resistance under loading and a decrease in the unloading phase, with the increase in resistance attributed to irreversible permanent damage [23]. Wen and Chung [24] published the first theoretical study on the phenomenon of strain sensitivity in fiber-reinforced cementitious materials in 2006, ascribing it to the piezoresistivity caused by the slight pull-out of fibers passing through microcracks.

With the development of nanotechnology in the last 10 years, the interest in studying electrical phenomena in materials containing conductive nanoparticles grew appreciably and increasing attention was devoted to the issue of dispersing the nanoparticles in a matrix [25].

Studies on the effect of nanoparticles in the form of nano-SiO_2 and nano-Fe_2O_3 added to mortar and concrete were carried out in [26–29]. The crack opening resulting from a compressive force caused the modification of an electric circuit and by extension the electrical resistance. Cementitious materials were studied with the addition of carbon nanofibers, nano-carbon black [29] and carbon nanotubes, in which the particles modified the electrical resistivity of concrete due to the piezoelectric effect [28]. The electrical properties of these smart nanofiber-reinforced cementitious materials were studied under different compressive stresses and loading–unloading cycles. Other researchers also evaluated the influence of hybrid nanoreinforcements, such as combination of carbon fibers and carbon nanotubes, on the self-sensing properties of cement-based sensors [30].

The results of the literature works indicate that, under static or slow cyclic loading, fiber-reinforced cement-based sensors show a good correlation between resistivity changes and load changes. This property makes them suitable for SHM applications. Studies also show that carbon nanotubes in cement-based sensors provide better strain sensibility and fidelity when compared to other nanoparticles.

Cement-based materials possess dielectric properties, causing them to exhibit the effects of polarization. Polarization occurs when a dielectric is subjected to an electric field. The applied electric field polarizes the material by orienting the dipole moments of molecules that have random orientations under normal conditions. The result of polarization is an electric field in the direction opposite to the applied electric field due to the formation of the dipoles [31]. The polarization therefore causes an increase in electrical resistance during measurement [32]. Moreover, higher conductivity in the material causes a lower tendency to polarize.

3. Motivations and objectives of the work

The literature review reveals that the strain-sensing ability of cement-based materials with carbon nanoparticles has been mainly investigated under slowly-varying loads. On the contrary, almost unexplored is the electrical response of such materials when subjected to dynamic loads, with the few works devoted to this matter referring to (i) non-cement-based composites [33], (ii) cement-based composites with non-carbon nanoparticles [34] or (iii) cement-based materials with carbon nanoparticles considering relatively slow loading rates compared to typical rates of dynamic phenomena in civil engineering structures [30].

This work is aimed at exploring the possible application of carbon nanotube–cement composites for manufacturing transducers able to provide dynamic measurements of strain in the typical frequency range of vibration of large civil engineering structures. The development of cement-based sensors capable of measuring dynamic response quantities is indeed an important future research direction for the motivations that are briefly discussed below.

The main motivation for extending the study of strain-sensing capability of nanotechnology-modified cement-based materials to the dynamic range is to find fruitful applications in dynamic SHM, which is currently seen as a major research subject in civil engineering whose main purpose is the early assessment of structural damage using global dynamic measurements. Moreover, such materials might be even better suited for dynamic measurements than for static ones because disturbances resulting from slow nonlinear phenomena, beginning with the polarization of a material, could, in principle, be greatly reduced in the dynamic range with rapidly varying strains, making the task of interpreting the sensors' output easier.

Nanotechnology-modified cement-based sensors promise significant advances with respect to traditional ones commonly used for dynamic monitoring and feedback control [35–38] such as accelerometers and electric strain gauges. The most interesting feature of cement-based sensors is their possibility of being naturally embedded inside the structural core by using a sensor material similar to that of the structure. This concept encourages the transformation of structures themselves into infinite sets of potential sensors, thus enlarging the sensitive volume to its maximum extent. Naturally, the actual number of sensors is determined by the distance of the electrodes. Such compatibility between sensors and structure is impossible with traditional contact sensors that are always externally "attached" to the monitored structure and wired to data acquisition systems.

Another important advantage of cement-based sensors would be their enhanced durability with respect to traditional sensors, whose service lives are generally short. These aspects are timely due to the current trend towards time-continuous dynamic monitoring applications where structural health assessment is unbiased by variations in environmental conditions, such as air temperature and humidity.

Furthermore, cement-based smart sensors would, in principle, retain all the features of traditional electric strain gauges, overcoming the well-known difficulties in the evaluation of displacement time histories from the acceleration records provided by traditional accelerometers [39,40].

The applications of cement-based smart sensors would cover most cases of interest in the SHM of large concrete structures, such as tall buildings, bridges, dams and more, in which traditional testing techniques based on local inspections can become especially troublesome due to the structures' large spatial extents and the use of traditional dynamic sensors becomes almost prohibitive because of maintenance and access difficulties.

4. Experimental procedures

A set of experiments was performed to investigate the dynamic response of cement-based sensors. The tests aimed to investigate the sensitivity of cement paste specimens prepared with carbon nanotubes to deformation determined by applied dynamic loads and were based on the measurement of electric current between two points of the samples subjected to a fixed potential difference. The following sections present the specimens' characteristics, techniques adopted for dispersing the nanotubes, experimental setup and experimental procedures.

4.1. Material and specimens' characteristics

Cement paste prismatic specimens with dimensions of $40 \times 40 \times 160$ mm were made using cement type 42.5 and Arkema Multi-Wall Carbon Nanotubes (MWCNTs), type Graphistrength C100. The electrical connections were made using two 1 mm-diameter copper wires directly embedded in the center of the samples at a mutual distance of 40 mm. Bidimensional probes, such as plates or nets, where not considered in order not to reduce the mechanical strength of the cross-section of the specimens.

The choice of cement paste for constructing the specimens was motivated by the understanding that such a cementitious material is more homogeneous and potentially more strain-sensitive than cement mortar or concrete because it lacks sand and stone aggregates.

The relevant properties of the nanotubes used in these specimens are summarized in Table 1. Multi-wall carbon nanotubes were adopted because they are more sensitive to stress changes than single-wall nanotubes. This enhanced sensitivity was motivated by the higher probability of having a greater number of contact points that would determine a more significant decrease in the cementitious material's electrical resistivity with the strain.

Table 1
Properties of the MWCNTs used in the experiment.

Property	Description/Value
Appearance	Black powder
Apparent density	50–150 kg/m^3
Mean agglomerate size	200–500 μm
Weight loss at 105 °C	<1%
Carbon content	>90% In weight
Free amorphous carbon	Undetectable (SEM)
Mean number of walls	5–15
Outer mean diameter	10–15 nm
Length	0.1–10 μm

Table 2
Cement paste mix design.

Components	Content
MWCNTs	32.4 kg/m^3
Cement type 42.5	1620 kg/m^3
Superplasticizer	32.4 dm^3/m^3
Water	650 kg/m^3
w/*c* Ratio	0.4

The composition of the cement paste is shown in Table 2. The carbon nanotubes used for the samples were in the amount of 2% by weight of cement. The fabrication procedure of MWCNTs reinforced cement-based material was divided into two steps: first, the dispersion of nanotubes in aqueous solution with the mechanical and physical methods reported below, and second, the addition of cement by typically mixing methods for conventional cement-based materials.

4.2. Technique used for dispersing the nanotubes into water

Nanoparticles tend to agglomerate due to their small dimensions, and the process of adding these particles to the cement mix proved to be a delicate task.

The dispersion of the nanoparticles in the cement matrix was accomplished in two phases. In the first phase, the nanoparticles were spread in water and the obtained water suspension was added to the cement powder in the second phase.

The addition of the nanotubes to deionized water was performed with a magnetic stirrer, a mechanical agitator and by sonication. The power of the sonicator's ultrasounds was adjusted to 225 W.

The agitator's speed of rotation was set to 1500 rev/min. The sonication and mechanical mixing of the carbon nanotubes in deionized water lasted 15 min, allowing for proper dispersion with limited water evaporation caused by overheating from the mixer. After mixing, the water solution with nanotubes was combined with cement to create the paste.

The control of the effective dispersion of nanoparticles in the aqueous solution and in the cement paste was performed using a scanning electron microscope (SEM) (type FESEM, model Supra 25, Zeiss) with a field emission cathode. SEM analyses of water solution with MWCNTs after the mixing process and of hardened cementitious material were performed. The images demonstrate the effectiveness of the mixing process showing the good nanotubes' dispersion in water (Fig. 1a) and in cement paste after curing (Fig. 1b).

4.3. Experimental set up

To investigate the dynamic properties of the cement-based sensors, an experimental procedure was performed that considered

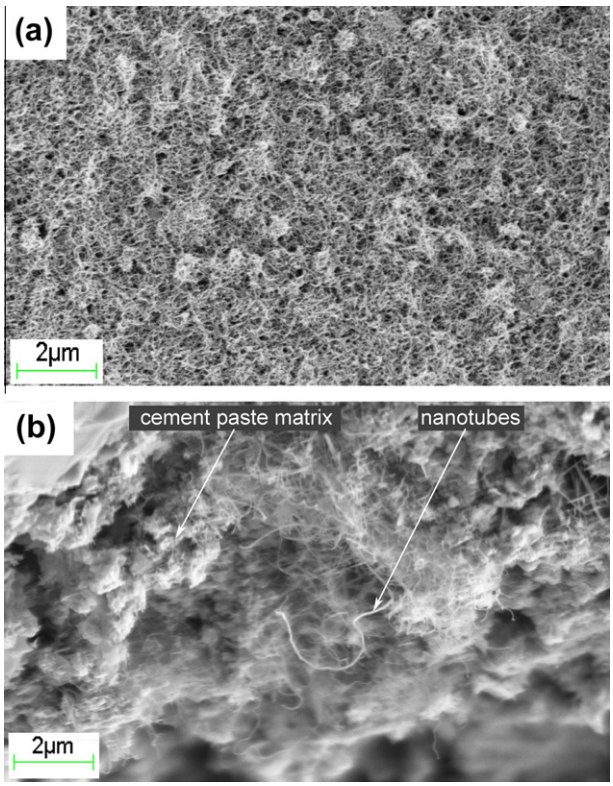

Fig. 1. SEM images: MWCNTs-water solution, Mag = 50.00 kX (a); sample of cement paste with MWCNTs, Mag = 25.00 kX (b).

sinusoidal compression loads and corresponding axial deformations as the inputs and measurements of electrical resistance as the outputs.

The application of the axial load to the cement paste samples was accomplished with a hydraulic press (type MTS Model 243.40T) operating under force control. A PC-controlled acquisition system was used to measure the applied load values with a MTS Force Transducer Model 661.23F-01 and record the axial deformation of the cement paste at mid-height with strain gauges positioned on the lateral surfaces of opposite faces. The measured values were sampled with a Spider8 device. An electrometer (Keithley mod. 6517B with resistivity test fixture mod. 8009) with its acquisition system connected to the two copper electrodes was used to measure electric current with an applied voltage of 30 V. The two-probe method was thus used (Fig. 2) where the same copper electrodes served both for applying voltage difference and for measuring current intensity. The electrodes were embedded in the specimens to ensure a good connection with the sensing material. It is worth mentioning that some authors [27,31] preferred to use the four-probe method where the voltage difference was applied at two outer electrodes, while inner electrodes were used only for measuring. A similar procedure was not implemented in this work because, considering the high resistivity of the material, an increase in the distance of the active electrodes would have resulted in very low current intensities, hard to be measured at sufficient sampling rates to investigate dynamic phenomena. On the other hand, the distance between the two copper electrodes could not be reduced below 4 cm in order to satisfy the analogy with strain gauges used in concrete structures. However, future developments of this work shall explore different test configurations, such as the four-probe method using plates or net metallic probes, possibly by further improving material properties, sensors' sensitivity or by using signal conditioning techniques.

4.4. Experimental tests

First of all, experiments with quasi-static cyclic variations of axial compression loads were conducted with the purpose of obtaining the stress–strain constitutive relation of the specimens in the state of elastic reversible deformation. The results are presented in Fig. 3, with strain ϵ (average between the two strain gauges) expressed in millistrain ($m\epsilon$) units, and demonstrate that the stress–strain relation was non-linear in the very low stress-amplitude range. From a quadratic interpolation of the measured stress–strain curve, the tangent Young modulus of the cement paste was estimated and is also shown in Fig. 3.

In a second stage of experimental tests, dynamic investigations were performed in the frequency range 0.1–5 Hz, covering the typical frequency content of the dynamic response of large civil engineering structures. Two types of tests were included in the study. Test type *a* measured the specimens' responses to sinusoidal compression loads, and test type *b* measured responses to axial loads with sweep variation of the frequency.

The tests were conducted after the application of a constant potential difference of 30 V, without any load, for 1000 s to reduce the polarization effect.

A total of 16 type *a* tests were performed, each one characterized by a different load frequency value, from 0.1 to 1.0 Hz with step increments of 0.1 Hz, from 1.0 to 3.0 Hz with step increments of 0.5 Hz, and from 3.0 to 5.0 Hz with step increments of 1.0 Hz.

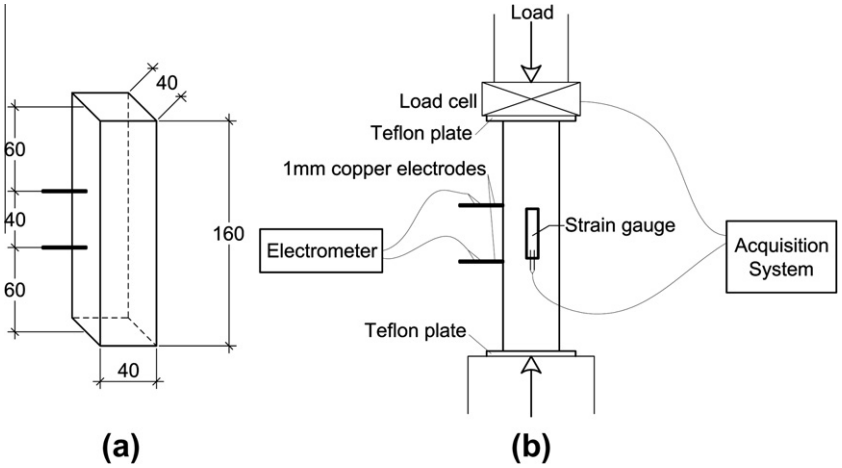

Fig. 2. Sketch of the sensor (a) and of the measurement system (b) with dimensions in mm.

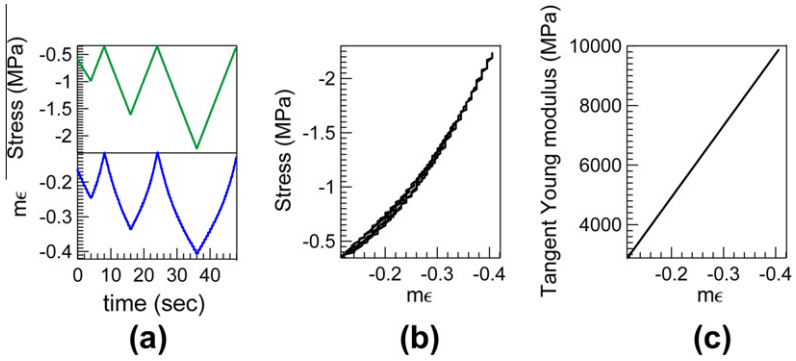

Fig. 3. Measured stress–strain constitutive relationship of the sensors: time-history results of stress and strain (a); stress–strain curve (b); and tangent Young modulus vs. strain (c).

Each type *a* test consisted of applying a constant compression load of 2 kN for a duration of 240 s followed by sinusoidal loads with intensity varying from 2 kN to 4 kN and corresponding to axial stresses of 1.25 MPa and 2.5 MPa, respectively. The values of applied stresses were chosen to investigate the electrical response of the sensors in the elastic uncracked state. The total duration of each type *a* test was 360 s for frequencies less than or equal to 1.0 Hz and at least 300 s for higher frequencies.

The load and axial strain were measured at a sampling frequency of 10 Hz when the frequency of the load was less than or equal to 1.0 Hz and 25 Hz at higher frequencies. The current intensity was recorded at the maximum sampling frequency compatible with the accuracy required for similar low-level measurements. In fact, increasing sampling rate resulted in reducing accuracy and increasing measurement noise. After preliminary testing, which is not reported here for the sake of brevity, the sampling frequency was set at 13.5 Hz. The electrical resistance was evaluated by dividing the applied voltage (30 V) by the measured current.

The type *b* tests consisted of the initial application of a constant compression load equal to 2 kN (axial stress equal to 1.25 MPa) for 70 s followed by concatenated sinusoidal compression loads with different frequencies and amplitudes varying from 2 kN to 4 kN (axial stress varying between 1.25 MPa and 2.5 MPa). In all, 10 load cycles were applied at 14 different load frequency values: from 0.1 to 0.5 Hz with step increments of 0.1 Hz, 0.75 Hz, from 1.0 to 4.0 Hz with step increments of 0.5 Hz, and 5.0 Hz. Two separate tests were performed, one with increasing frequencies (forward sweep test) and one with decreasing frequencies (backward sweep test). The total duration of each type *b* test was approximately 340 s.

The loads and strains in the type *b* tests were sampled at 25 Hz, while the current intensity was sampled at 13.5 Hz.

5. Dynamic properties of the sensors

5.1. Natural frequency of the sensors

To avoid significant amplification phenomena within the frequency working range, the sensors were designed to have a natural vibration frequency similar to that of the acceleration transducers commonly used in civil engineering applications. The natural vibration frequency of the sensors, f_0, was estimated using a well-known formula for the axial vibration of continuous rods:

$$f_0 = \frac{1}{2L}\sqrt{\frac{E}{\rho}} \tag{1}$$

where L is the length of the sensor, E is its Young's modulus and ρ is the mass density.

Eq. (1) is valid assuming a linearly elastic material, fixed axial displacements at both ends of the specimen and modeling the sensor as a monodimensional element. It should be noticed that none of these hypotheses fully applies in the presented case because, as shown in the results of Fig. 3, the material used for the sensor is characterized by a nonlinear constitutive relation, actual boundary conditions might be different from ideal ones and the assumption of monodimensionality does not apply considering the aspect ratio of the prismatic specimens. However, Eq. (1) can be regarded as a rough approximation of the natural frequency of the sensors which is useful for estimating at least its order of magnitude. In particular, in the present case, assuming a tangent Young modulus equal to 7000 MPa, corresponding to the value measured at an axial stress of 1.25 MPa, and using the measured value for ρ, equal to 1680 kg/m^3, Eq. (1) yields $f_0 = 6.4$ kHz which is suitable for the applications under study.

5.2. Response to sine waves

Fig. 4 shows the full-length time histories of applied stress, measured strain and measured electrical resistance R for a frequency of 0.1 Hz. Fig. 5 shows window plots of the time histories during the application of sinusoidal loads.

The electrical resistance in Fig. 4 increases during the application of a constant load because of the slow polarization of the cement paste prepared with carbon nanotubes. It should be also noted that the initial value of the electrical resistance depended upon the sensor's initial level of polarization and, for this reason, different time histories of measured electrical resistance in Fig. 5 started from different initial values.

Because the initial quantity of charge of the specimens was unknown, an initial reference value for electrical resistance was lacking and, consequently, the adopted measurement technique did not allow obtaining the absolute strain value from measured elec-

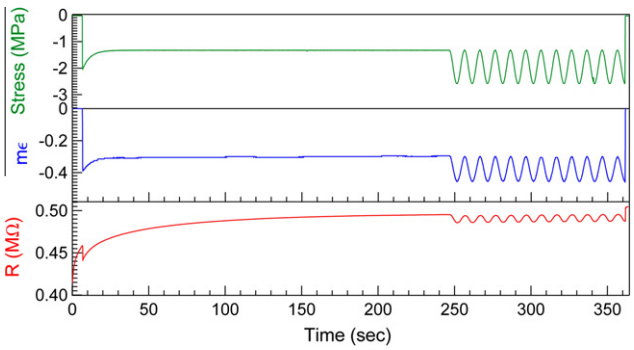

Fig. 4. Axial stress, measured strain and measured electrical resistance vs. time for a load frequency of 0.1 Hz.

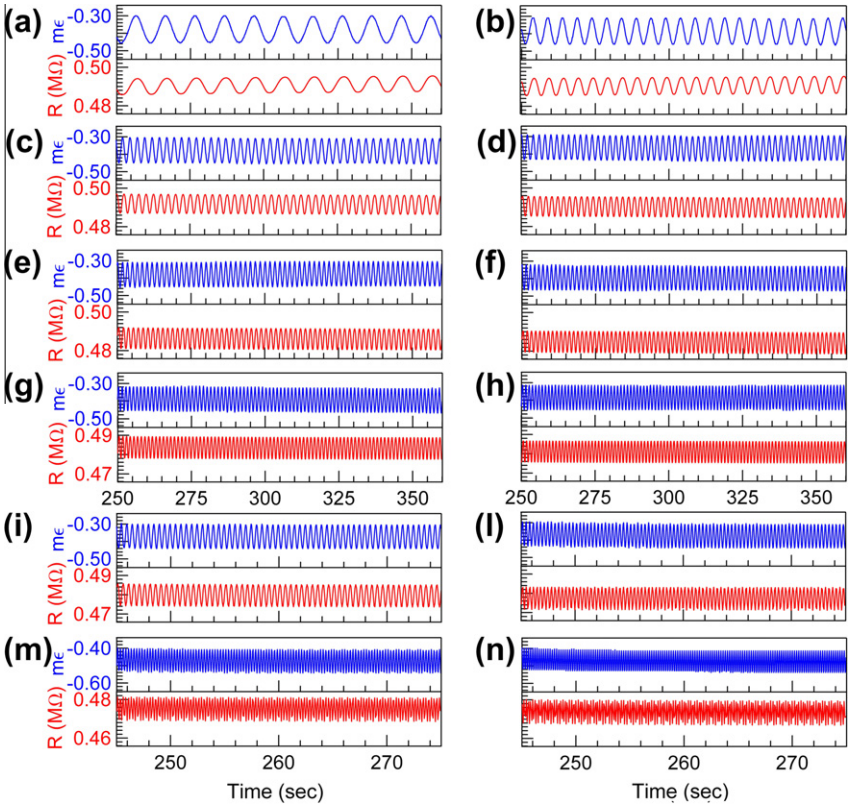

Fig. 5. Measured strain and electrical resistance vs. time for different load frequencies: 0.1 Hz (a); 0.2 Hz (b); 0.4 Hz (c); 0.5 Hz (d); 0.6 Hz (e); 0.7 Hz (f); 0.8 Hz (g); 0.9 Hz (h); 2.0 Hz (i); 3.0 Hz (l); 4.0 Hz (m); and 5.0 Hz (n).

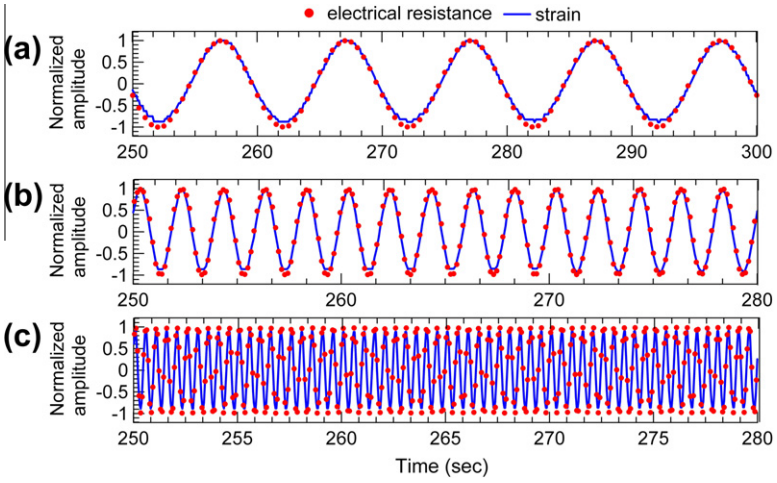

Fig. 6. Normalized measured strain and electrical resistance vs. time for different load frequencies: 0.1 Hz (a); 0.5 Hz (b) and 2.0 Hz (c).

trical response of the sensors. It should be noticed, however, that a similar information is not essential in dynamic applications where variations of mechanical quantities around a mean value are concerned while the mean value itself is either zero, such as in the case of acceleration measurements, or unknown, such as in the case of strain measurements.

Similarly to what found in other literature works [8,27,30], the application of a compression load produced a decrease in electrical resistance that was visible in the initial loading phase and the subsequent dynamic phase.

Good correlation was qualitatively observed between axial strain and electrical resistance during the applications of sinusoidal load shown in Figs. 4 and 5, although the effects of sampling errors became significant in the time histories of electrical resistance for frequencies higher than 2.5 Hz. It should be noticed that the loading rates corresponding to the applied sinusoidal loads were remarkably larger than those adopted in other literature works on similar materials [30]. The results can thus contribute to extend the known strain-sensing capability of carbon nanotube–cement composites to the dynamic range.

To better highlight the correlation between axial strain and electrical resistance, some of their time histories are plotted together in Fig. 6 after elimination of the mean value and normalization to a unit peak value. The mean value was eliminated from

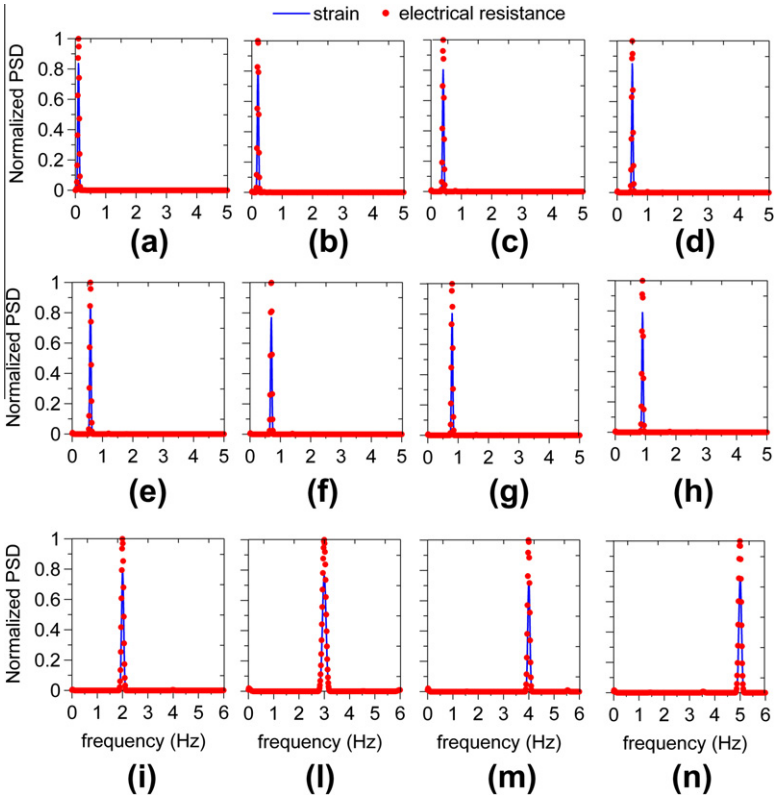

Fig. 7. Normalized PSD of strain and electrical resistance for different load frequencies (Hz): 0.1 Hz (a); 0.2 Hz (b); 0.4 Hz (c); 0.5 Hz (d); 0.6 Hz (e); 0.7 Hz (f); 0.8 Hz (g); 0.9 Hz (h); 2.0 Hz (i); 3.0 Hz (l); 4.0 Hz (m); and 5.0 Hz (n).

the time history signals of electrical resistance by subtracting a function obtained as the average of two cubic splines interpolating the maximum and minimum peaks from the original signals.

The results presented in Fig. 6 clearly show that the normalized input and output are almost perfectly overlapped. The remaining test results, omitted for the sake of brevity, yielded the same conclusion.

Fig. 7 shows the power spectral density (PSD) functions of the quantities plotted in Fig. 6. The PSD functions were also normalized to a unit maximum value, keeping the ratio between the amplitudes of the leading peak of the PSD of the input and those of the PSD of the output fixed.

The results in Fig. 7 show that the response frequency coincides with the strain frequency, indicating a good match between the input and output PSDs. Slight differences in peak amplitudes were observed that may have been somewhat enhanced by sampling errors.

5.3. Response to frequency sweep tests

The results of the tests with forward and backward sweep frequencies are plotted in Fig. 8. The effect of the material's slow polarization is again visible in the phase with applied constant load.

The results presented in Fig. 8 show, at first glance, that the sensor response during the application of the sinusoidal loads with frequency sweep was always well correlated with the strain. However, some variations of the amplitude and mean value of the electrical response over time are also visible in Fig. 8. In particular, the mean value of the electrical resistance decreased over time in the forward sweep test, but increased over time in the backward sweep test. This behavior not only was associated with the polarization of the material (otherwise an increasing trend would have been observed in both tests) but also highlighted a slight frequency dependency of the mean value of the electrical resistance.

The amplitude of the electrical response in Fig. 8 is also frequency-dependent. In fact, the amplitude increased with the frequency in both the forward and backward sweep tests: this result well agrees with the loading-rate dependency of the fractional change in resistivity observed in [30].

For a more in-depth analysis of the sweep test results, Fig. 9 shows the overlapped time histories of strain and electrical resistance with normalized amplitudes, where the signal recorded by the electrometer has been previously treated by removing the best straight line linear trend. The two curves in Fig. 9 confirm that the electrical resistance is well correlated with the axial strain even at relatively high loading frequencies.

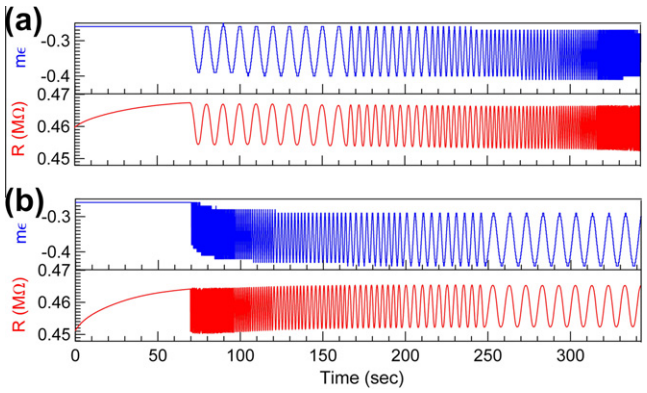

Fig. 8. Measured strain and electrical resistance vs. time: test with forward sweep of the frequency from 0.1 Hz to 5.0 Hz (a) and test with backward sweep of the frequency from 5.0 Hz to 0.1 Hz (b).

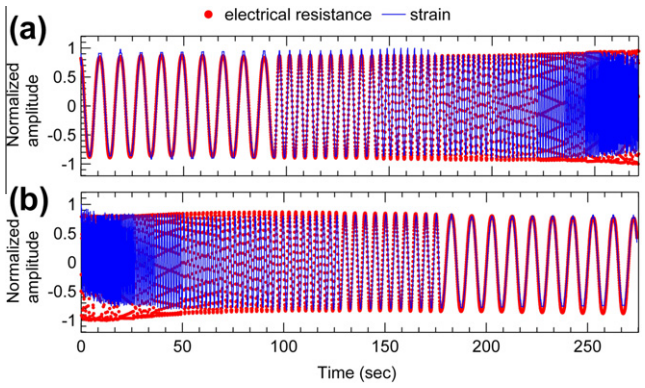

Fig. 9. Normalized measured strain and measured electrical resistance vs. time: test with forward sweep of the frequency from 0.1 Hz to 5.0 Hz (a) and test with backward sweep of the frequency from 5.0 Hz to 0.1 Hz (b).

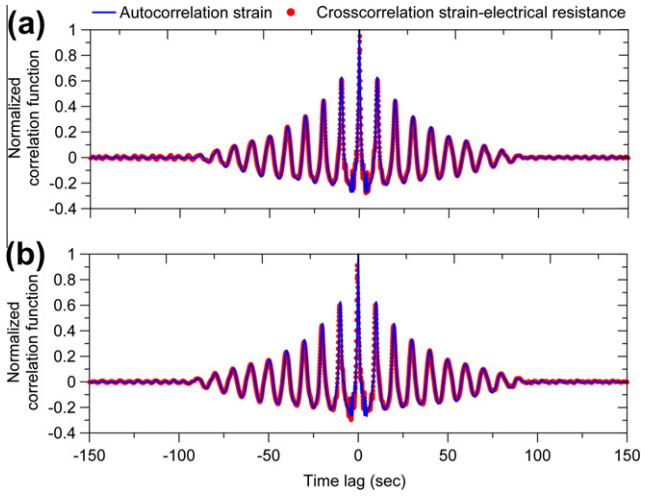

Fig. 10. Autocorrelation of normalized strain and crosscorrelation between normalized strain and normalized electrical resistance: test with forward sweep of the frequency from 0.1 Hz to 5.0 Hz (a) and test with backward sweep of the frequency from 5.0 Hz to 0.1 Hz (b).

The good correlation between strain and electrical resistance is quantitatively highlighted in Fig. 10, which shows the autocorrelation function of the recorded axial strain and the cross-correlation function between the axial strain and electrical resistance. These two quantities were satisfactorily overlapped in both the forward and backward sweep tests.

The measurement of the axial strain through the strain gauges also allowed estimating the gauge factor (GF) of the cement-based sensors. The GF is defined as:

$$GF = \frac{\Delta R/R_0}{\Delta \epsilon} \tag{2}$$

where ΔR is the amplitude of the measured electric resistance, R_0 is its mean value and $\Delta\epsilon$ is the amplitude of the measured strain (average between the two strain gauges). During the tests *GF* proved to be increasing with frequency as found in other literature works [30]. An average value of $GF = 220$ was obtained within the investigated frequency range.

5.4. Estimation of the frequency response function of the sensors

The dynamic characteristics of a transducer governed by a linear input–output differential equation are fully described by its frequency response function (FRF) which is a complex function defined as:

$$FRF(f) = \frac{Y(f)}{X(f)} \tag{3}$$

where $Y(f)$ is the Fourier Transform of the output response $y(t)$, $X(f)$ is the Fourier transform of the input $x(t)$, t denotes time and f denotes frequency. If the input is harmonic with the form $x(t) = X_0 \cdot cos(2\pi f\, t)$, where X_0 is the input amplitude, the stationary output, after an initial transitory, is also harmonic with the following form:

$$y(t) = Y_0(f)cos(2\pi ft + \phi(f)) \tag{4}$$

where $Y_0(f)$ is the output amplitude and $\phi(f)$ is the phase shift between input and output. The amplitude of $FRF(f)$, Eq. (3), coincides with the ratio between $Y_0(f)$ and X_0:

$$|FRF(f)| = \frac{Y_0(f)}{X_0} \tag{5}$$

while $\phi(f)$ coincides with the phase of $FRF(f)$.

The dynamic response of transducers commonly used for vibration measurements is often described through a second-order differential input–output equation. In this case the *FRF* only depends upon the resonant frequency of the sensor and its damping. When the excitation frequency is much smaller than the resonant frequency of the sensor, the FRF can be approximated with a constant function with zero phase, which corresponds to the response of a perfect transducer characterized by an ideal linear input–output relation without delay. Furthermore, when the excitation frequency is much smaller than the resonant one, as it is the case, the error that is committed by approximating the FRF with a constant function is essentially independent of the damping.

The results of the sweep tests were used for further investigating the dynamic response of the sensors by estimating the amplitude of its FRF using Eq. (5). In particular, the FRF was calculated for each value of the excitation frequency as the ratio between the amplitude of the measured electrical resistance and that of the applied axial load. At first, the best-fitting linear trend was removed from the full-length records after the initial 70 s. Next, each time window with 10 cycles at constant frequencies was extracted, and the average peak-to-peak amplitude of both electrical resistance and applied load were evaluated. Finally, the FRF was obtained as the ratio between the amplitude of the output and that of the input. Normalization of the FRF was accomplished by dividing it by the value corresponding to the lowest frequency (0.1 Hz).

The results are shown in Fig. 11 for the interval 0.1–3.5 Hz. The FRF was not evaluated for frequencies higher than 3.5 Hz because sampling errors became unacceptable in this range (the sampling

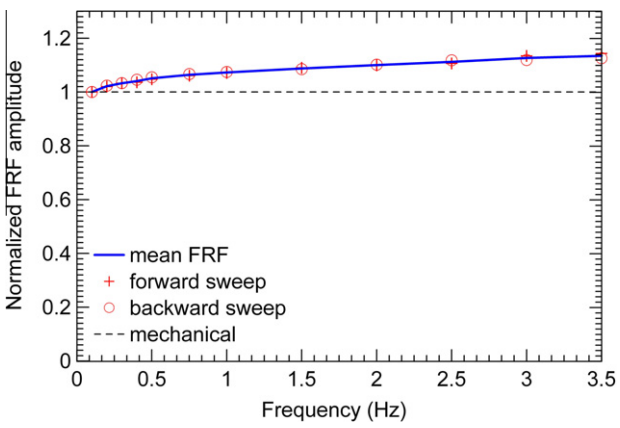

Fig. 11. Measured frequency response curve of the sensors.

rate of 13.5 Hz did not allow for an accurate description of the sinusoidal signals with frequencies higher than 3.5 Hz). On the contrary, the comparison between the FRF extracted from forward and backward sweep responses in the range below 3.5 Hz showed a satisfactory match implying that the errors associated with the elimination of the trend from the time histories and the sampling were limited in this range.

For comparative purposes, Fig. 11 also shows the mechanical FRF that would result from ideal behavior of the sensors modeled as second-order systems with natural frequency equal to f_0, Eq. (1). This function was evaluated by assuming a critical damping ratio equal to 0.01 that can be considered as representative of the internal damping of hardened cement paste in its uncracked state [41].

The results presented in Fig. 11 confirm the initial prediction of a slight amplitude increase of the response with the frequency, especially in the low-frequency range. This result implied that the sensors were characterized by a weakly non-linear input–output relation. It should be noted that this phenomenon did not result for mechanical reasons because, as shown in Fig. 11, the mechanical FRF was perfectly straight in the investigated frequency range as a consequence of the high natural frequency of the sensors. On the contrary, it must be ascribed to the peculiar electrodynamic behavior of the cement paste prepared with carbon nanotubes in this study. It should be noted that, because of the high natural frequency of the sensors, a straight mechanical FRF would have been obtained in the low frequency range shown in Fig. 11 independently from the assumed value of material's internal damping.

Although the distortion introduced by the slightly increasing FRF could be corrected by appropriately filtering the measured outputs using a model for the FRF (for instance a power law which seems to be suitable to describe the FRF amplitude vs. frequency), it is worth noting that, in the range of 0.1–3.5 Hz, the dynamic error that would have resulted from assuming a constant FRF was on the order of ±5%, which is acceptable for most applications and ambient vibration structural tests aimed at modal identification.

6. Conclusions

The paper presented an investigation on the dynamic response of prismatic specimens composed of cement paste prepared by adding multi-wall carbon nanotubes. The study aimed to develop cement-based nanotechnology-modified sensors for possible application in dynamic response measurements and structural health monitoring of concrete structures.

After presenting an appropriate technique for obtaining good dispersion of carbon nanotubes in cement paste, experimental tests were conducted to measure the change in electrical resistance of the specimens when subjected to sinusoidal compression loads. The cement paste always remained in the linear elastic range of deformation during the tests and the typical frequency content of large civil structures, such as bridges and tall buildings, was covered by the range of frequencies tested.

The results of the experimental tests demonstrated that a sinusoidal compression load as input produced a sinusoidal variation of the electrical resistance as output which, as the load frequency was increased, was progressively less affected by polarization phenomena. Moreover, input and output frequencies were almost identical over the entire investigated frequency range. Hence, this type of sensors seems to be particularly interesting for dynamic measurements.

Tests with sweep variation in the axial load frequency allowed a more in-depth study of the specimens' dynamic response. A very close correlation was observed between the measured electrical resistance and the axial strain. Moreover, the results of the sweep tests allowed the researchers to obtain an approximation of the sensors' frequency response function that outlined a quasi-linear relationship between the input and output. A slightly increasing frequency response function was noted, the slight nonlinearity of which was probably associated with the effects of polarization phenomena at low frequencies. In fact, the frequency response function tended to show ideally linear behavior as the load frequency increased, which confirms that the sensors are apt to measure rapidly varying strain responses.

Based on the results obtained in this study, the investigated specimens can be considered prototype sensors that appear to be suitable for performing dynamic measurements in civil engineering concrete structures.

References

[1] D'Alessandro A. The use of the nanotechnologies for the realization of cementitious materials sensitive to the state of strain, PhD thesis. Perugia, University of Perugia; 2012.
[2] Mondal P, Shah SP, Marks LD. Nanoscale characterization of cementitious materials. ACI Mater J 2008;105:174–9.
[3] Kovler K, Roussel N. Properties of fresh and hardened concrete. Cem Concr Res 2011;41(7):775–92.
[4] Chen PW, Chung DDL. Carbon fiber reinforced concrete for smart structures capable of non-destructive flaw detection. Smart Mater Struct 1993;2:22–30.
[5] Chen P, Chung DDL. Concrete as a new strain/stress sensor. Compos Part B–Eng 1996;27:11–23.
[6] Fu X, Chung DDL. Self-monitoring of fatigue damage in carbon fiber reinforced cement. Cem Concr Res 1996;26(1):15–20.
[7] Fu X, Ma E, Chung DDL, Anderson WA. Self-monitoring in carbon fiber reinforced mortar by reactance measurement. Cem Concr Res 1997;27(6):845–52.
[8] Chung DDL. Cement reinforced with short carbon fibers: a multifunctional material. Compos Part B–Eng 2000;31:511–26.
[9] Fu X, Lu W, Chung DDL. Improving the strain-sensing ability of carbon fiber-reinforced cement by ozone treatment of the fibers. Cem Concr Res 1997;28(6):183–7.
[10] Kollosche M, Stoyanov H, Laflamme S, Kofod G. Strongly enhanced sensitivity in elastic capacitive strain sensors. J Mater Chem 2011;21:8292–4.
[11] Monti M, Natali M, Kenny JM, Torre L. Carbon nanofibers for strain and impact damage sensing in glass fiber reinforced composites based on an unsaturated polyester resin. Polym Compos 2011;32(5):766–75.
[12] Laflamme S, Kollosche M, Connor JJ, Kofod G. Soft capacitive sensor for structural health monitoring of large-scale systems. Struct Control Health Monit 2012;19:70–81.
[13] Cohen DJ, Mitra D, Peterson K, Maharbiz MM. A highly elastic, capacitive strain gauge based on percolating nanotube networks. Nano Lett 2012;12:1821–5.
[14] Muto N, Yanagida H, Nakatsuji T, Sugita M, Ohtsuka Y, Arai Y. Design of intelligent materials with self-diagnosing function for preventing fatal fracture. Smart Mater Struct 1992;1:324.
[15] Meehan DG, Wang S, Chung DDL. Electrical-resistance-based sensing of impact damage in carbon fiber reinforced cement-based materials. J Intell Mater Syst Struct 2010;21:83–105.
[16] Wen S, Chung DDL. Uniaxial tension in carbon fiber reinforced cement, sensed by electrical resistivity measurement in longitudinal and transverse directions. Cem Concr Res 2000;30:1289–94.
[17] Wen S, Chung DDL. Damage monitoring of cement paste by electrical resistance measurement. Cem Concr Res 2000;30:1979–82.
[18] Wen S, Chung DDL. Uniaxial compression in carbon fiber-reinforced cement, sensed by electrical resistivity measurement in longitudinal and transverse directions. Cem Concr Res 2001;31:297–301.
[19] Wen S, Chung DDL. Defect dynamics of cement paste under repeated compression studied by electrical resistivity measurement. Cem Concr Res 2001;31:1515–8.
[20] Wen S, Chung DDL. Piezoelectric cement-based materials with large coupling and voltage coefficients. Cem Concr Res 2002;32:335–9.
[21] Wen S, Chung DDL. Strain-sensing characteristic of carbon fiber-reinforced cement. ACI Mater J 2005;102(4):244–8.
[22] Wen S, Chung DDL. Effects of strain and damage on strain-sensing ability of carbon fiber cement. J Mater Civ Eng 2006;18(3):355–60.
[23] Bontea DM, Chung DDL, Lee GC. Damage in carbon fiber-reinforced concrete, monitored by electrical resistance measurement. Cem Concr Res 2000;30:651–9.
[24] Wen S, Chung DDL. Model of piezoresistivity in carbon fiber cement. Cem Concr Res 2006;36:1879–85.
[25] Konsta-Gdoutos MS, Metexa ZS, Shah SP. Highly dispersed carbon nanotube reinforced cement-based materials. Cem Concr Res 2010;40(7):1052–9.
[26] Li H, Xiao H, Ou J. Effect of compressive strain on electrical resistivity of carbon black-filled cement-based composites. Cem Concr Comp 2006;28:824–8.

[27] Li H, Xiao H, Ou J. Effect of moisture on electrical properties of carbon black-filled cement composites. ACI Proc 2006;254:131–44.
[28] Li GY, Wang PM, Zhao X. Pressure-sensitive properties and microstructure of carbon nanotube reinforced cement composites. Cem Concr Comp 2007;29(5):377–82.
[29] Li H, Ou J. Smart concrete, sensors and self-sensing concrete structures. Key Eng Mater 2009;400–402:69–80.
[30] Azhari F, Banthia N. Cement-based sensors with carbon fibers and carbon nanotubes for piezoresistive sensing. Cem Concr Compos 2012;34:866–73.
[31] Wansom S, Kidner NJ, Woo LY, Mason TO. AC-impedance response of multi-walled carbon nanotube/cement composites. Cem Concr Comp 2006;28:509–19.
[32] Cao J, Chung DDL. Electric polarization and depolarization in cement-based materials, studied by apparent electrical resistance measurement. Cem Concr Res 2004;34:481–5.
[33] Loh KJ, Chang D. Zinc oxide nanoparticle-polymeric thin films for dynamic strain sensing. J Mater Sci 2011;46:228–37.
[34] Dong B, Xing F, Li Z. Electrical response of cement-based piezoelectric ceramic composites under mechanical loadings. Smart Mater Res 2011.
[35] Breccolotti M, Franceschini G, Materazzi AL. Sensitivity of dynamic methods for damage detection in structural concrete bridges. Shock Vib 2004;11(3–4):383–94.
[36] Breccolotti M, Gusella V, Materazzi AL. Active displacement control of a wind-exposed mast. Struct Control Health Monit 2007;14(4):556–75.
[37] Hong AL, Ubertini F, Betti R. Wind analysis of a suspension bridge: identification and finite-element model simulation. J Struct Eng–ASCE 2011;137(1):133–42.
[38] Ubertini F, Hong AL, Betti R, Materazzi AL. Estimating aeroelastic effects from full bridge responses by operational modal analysis. J Wind Eng Ind Aerodyn 2011;99:786–97.
[39] Thong YK, Woolfson MS, Crowe JA, Hayes-Gill BR, Jones DA. Numerical double integration of acceleration measurements in noise. Measurement 2004:36;73–92.
[40] Park KT, Kim SH, Park HS, Lee KW. The determination of bridge displacement using measured acceleration. Eng Struct 2005:27;371–378.
[41] Swamy N, Rigby G. Dynamic properties of cement paste, mortar and concrete. Mater Struct 1971;4(1):13–40.